The Astrophysical Journal, 679: L25–L28, 2008 May 20

NEW RESULTS ON THE SUBMILLIMETER POLARIZATION SPECTRUM OF THE ORION MOLECULAR CLOUD

John E. Vaillancourt,[1] C. Darren Dowell,[1,2] Roger H. Hildebrand,[3,4] Larry Kirby,[3] Megan M. Krejny,[5] Hua-bai Li,[6] Giles Novak,[5] Martin Houde,[7] Hiroko Shinnaga,[8] and Michael Attard[7]

Received 2008 March 24; accepted 2008 April 9; published 2008 April 24

ABSTRACT

We have used the SHARP polarimeter at the Caltech Submillimeter Observatory to map the polarization at wavelengths of 350 and 450 μm in a $\sim 2' \times 3'$ region of the Orion Molecular Cloud. The map covers the brightest region of the OMC-1 ridge including the Kleinmann-Low (KL) nebula and the submillimeter source Orion-south. The ratio of 450 to 350 μm polarization is $\sim 1.3 \pm 0.3$ in the outer parts of the cloud and drops by more than a factor of 2 toward KL. The outer cloud ratio is consistent with measurements in other clouds at similar wavelengths and confirms previous measurements placing the minimum of the polarization ratio in dusty molecular clouds at $\lambda \sim 350$ μm.

Subject headings: dust, extinction — ISM: clouds — ISM: individual (OMC-1) — polarization — submillimeter

1. INTRODUCTION

Studies of the wavelength dependence of interstellar polarization are common place in the near-visible region of the spectrum (e.g., Serkowski 1958; Martin & Whittet 1990; Martin et al. 1999; Whittet 2004). Such studies have put constraints on the mechanisms of magnetic grain alignment (Roberge 2004; Lazarian 2003, 2007) and the properties of dust grains responsible for interstellar extinction (e.g., Hildebrand & Dragovan 1995; Andersson & Potter 2007; Whittet et al. 2008 and references therein). There are fewer studies of the wavelength dependence at far-infrared and submillimeter wavelengths (~0.1–1 mm) where dust grains are responsible for most of the observed emission in Galactic clouds.

The first studies of multiwavelength far-infrared/submillimeter polarimetry found unexpected results. Rather than a featureless spectrum due to a single population of dust grains, the polarization spectrum is observed to fall from 60 to 100 to 350 μm before rising again to 850 and 1300 μm (Hildebrand et al. 1999; Vaillancourt 2002, 2007). This spectral structure is attributed to the existence of multiple dust grain populations whose polarizability or alignment efficiency is correlated with either the grain temperature, the spectral dependence of the emissivity (the "spectral index"), or a combination of both. However, the existing data are quite sparse in terms of both wavelength coverage and the types of objects observed (bright Galactic clouds). Therefore, rather than pursue observations with the ability to test specific physical models, our immediate goal is to improve the empirical description of the spectrum by measuring the polarization at additional wavelengths between 100 and 850 μm which bracket the observed minimum at 350 μm.

To further this goal we have begun a campaign to measure the polarization of Galactic clouds at both 350 and 450 μm using SHARP, the SHARC-II polarimeter at the Caltech Submillimeter Observatory. While this is a fairly short wavelength baseline, such measurements will further constrain the location of the polarization minimum. For example, one can simply ask whether the minimum is less than, greater than, or approximately equal to 350 μm. This will place additional constraints on the possible range of polarizations, temperatures, and emissivities of the constituent grain populations (e.g., Hildebrand & Kirby 2004).

We have carried out the first set of observations for this project toward the Orion Molecular Cloud (OMC-1), a bright and well-studied region of massive star formation (e.g., Houde et al. 2004; Johnstone & Bally 1999; Lis et al. 1998). In § 2 below we review the SHARP instrument and the polarimetric/photometric observations. Maps are presented in § 3 followed by a discussion of the polarization spectrum in § 4.

2. OBSERVATIONS AND DATA REDUCTION

SHARP (Li et al. 2006, 2008; Novak et al. 2004) is a foreoptics module that installs onto the SHARC-II camera. Incident radiation is split into two orthogonally polarized beams which are then imaged onto opposite ends of the 12×32 pixel^2 SHARC-II bolometer array. The result is a dual-polarization 12×12 pixel^2 polarimeter with a $55'' \times 55''$ field of view (FOV). The polarization is modulated by stepping a half-wave plate (HWP) at the relative angles 0°, 22.5°, 45°, and 67.5°.

Within each FOV and HWP position, standard photometric beam-switching was performed with a chop throw of $5'$ and a chop position angle in the range 80°–150° east of north. This is repeated at positions separated by $50''$ in right ascension and declination to build maps larger than the FOV. For this work we have generated maps of size $2' \times 3'$ encompassing the two brightest submillimeter cores in OMC-1 (the Kleinmann-Low nebula, hereafter KL; and the submillimeter source of Keene et al. [1982] sometimes called Orion-south, hereafter KHW). Observations at 350 and 450 μm were carried out on 2007 February 16 and 2006 December 5, respectively.

The generation of Stokes parameters, polarization amplitudes, and position angles within each single set of four HWP

[1] Division of Physics, Mathematics, and Astronomy, California Institute of Technology, MS 320-47, 1200 East California Boulevard, Pasadena, CA 91125; johnv@submm.caltech.edu, cdd@submm.caltech.edu.
[2] Also Jet Propulsion Laboratory.
[3] Enrico Fermi Institute and Department of Astronomy and Astrophysics, University of Chicago, 5640 South Ellis Avenue, Chicago, IL 60637; roger@oddjob.uchicago.edu, lkirby@oddjob.uchicago.edu.
[4] Also Department of Physics.
[5] Department of Physics and Astronomy, Northwestern University, 2145 Sheridan Road, Evanston, IL 60208; m-krejny@northwestern.edu, g-novak@northwestern.edu.
[6] Harvard-Smithsonian Center for Astrophysics, 60 Garden Street, MS-78, Cambridge, MA 02138; hli@cfa.harvard.edu.
[7] Department of Physics and Astronomy, University of Western Ontario, London, ON N6A 3K7, Canada; houde@astro.uwo.ca, mattard@uwo.ca.
[8] Caltech Submillimeter Observatory, 111 Nowelo Street, Hilo, HI 96720; shinnaga@submm.caltech.edu.

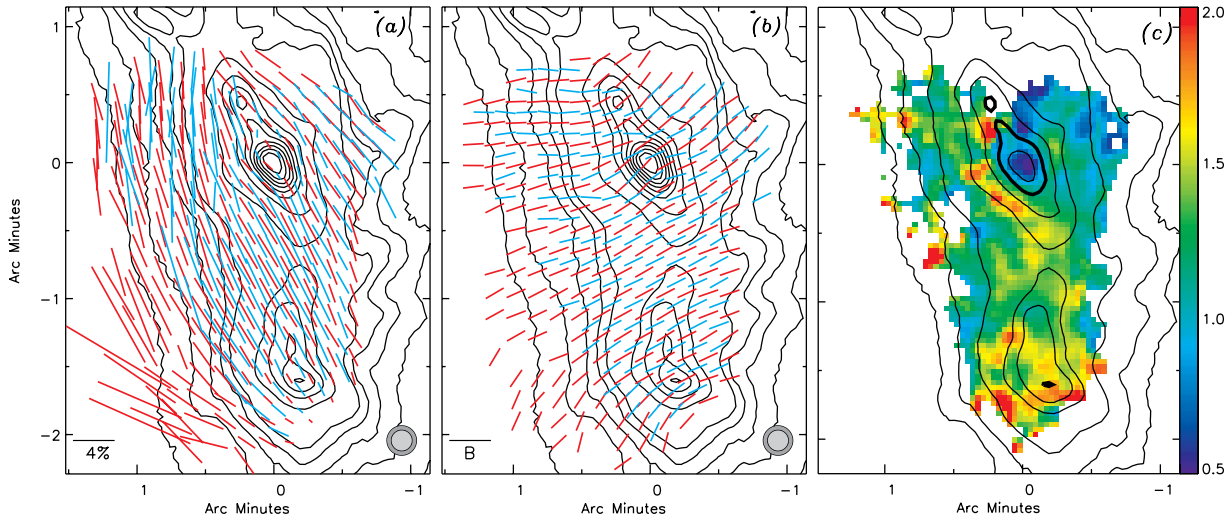

FIG. 1.—Polarimetric and photometric maps of OMC-1. Effective beam sizes (FWHM) for the photometric (9″) and polarimetric (13″) observations are shown as gray circles in (*a*) and (*b*). Coordinate offsets are measured with respect to Ori IRC 2 at $5^h35^m14.5^s$, $-5°22'31''$ (J2000.0). KL is the northernmost flux density peak coincident with the coordinate origin and KHW/Orion-south is the peak ∼1.5′ to the south. Only polarization data satisfying $P > 3\sigma_p$ are included. (*a*) 350 (*red*) and 450 (*blue*) μm polarization vectors superposed on 350 μm flux density contours. Contours are drawn at 2, 4, 6, 8, 10, 20, …, and 90 percent of the peak (≈780 Jy per 9″ beam). (*b*) Inferred magnetic field vectors at 350 and 450 μm drawn with a constant length (i.e., not proportional to the polarization amplitude); contours as in (*a*). (*c*) The color scale shows the polarization ratio between the two wavelengths, *P*(450)/*P*(350). Contours at 350 μm are drawn at 4, 6, 10, 20, 30, 50, and 80 percent of the peak flux density; the 50% contour is drawn thicker (see Fig. 4).

angles follows the same general procedures outlined by Platt et al. (1991) and Hildebrand et al. (2000). Maps of the linear Stokes parameters *I*, *Q*, and *U* are generated from the dithered and stepped array positions by interpolating the data onto a finer grid and co-adding (e.g., Houde & Vaillancourt 2007).

The polarization data presented in § 3 have been corrected for positive bias (Simmons & Stewart 1985; Vaillancourt 2006) and for measured polarization efficiencies of 93% and 98% at 350 and 450 μm, respectively. The data have also been corrected for instrument polarizations of ≈0.3%–0.5% at 350 μm and ≲0.2% at 450 μm (Li et al. 2008; J. E. Vaillancourt et al., in preparation). The polarization position angle calibration is accurate to within 2°.

We obtained photometric data at 350 μm using SHARC-II in camera mode on 2007 August 11–12. Four raster scans (without chopping) centered on Ori IRC 2 were performed to cover a ∼10′ × 10′ field. Maps were produced using the `sharcsolve`[9] utility, which models the source signal, sky background fluctuations, instrument gains, and drifts in the instrument electronics. Absolute flux densities are calibrated with respect to the standard sources L1551 and Mars (using peak flux density estimates of 45.2 and 3.80×10^3 Jy per 9″ FWHM beam, respectively)[10] and have an uncertainty of ∼20%.

3. RESULTS

Figure 1 shows the polarimetric and photometric maps in the ∼2′ × 3′ region covered by the polarization observations. The size of the Gaussian smoothing kernel used to interpolate the 350 μm polarization data has been chosen so that the resulting resolution matches that of the 450 μm polarization data (13″ FWHM). Figures 1*a*–1*c* plot the 350 and 450 μm polarization results over a contour map of total flux density measured at 350 μm.

Figure 1*a* shows the polarization results with the length of the vector proportional to the measured polarization amplitude and the position angle parallel to the polarization vector. The most obvious feature of this map is the decrease in the polarization amplitude (at both wavelengths) toward the KL intensity peak, and to a lesser extent toward KHW. This so-called polarization hole effect in which the polarization drops toward intensity peaks has been observed in these and other sources by experiments at a range of far-infrared and submillimeter wavelengths (e.g., Schleuning 1998; Coppin et al. 2000; Matthews et al. 2001; Dotson et al. 2000, 2008).

In Figure 1*b* we have rotated the polarization vectors by 90° to show the inferred magnetic field direction. The plotted ***B***-vectors are drawn with a constant length (not proportional to polarization amplitude) in order to more clearly observe the position angle differences across the map and between the two wavelengths. The position angles exhibit a clockwise rotation with increasing wavelength, differing by more than 25° around KL and the region immediately east. This angular rotation is much smaller to the west and south of KL. The larger variation of the position angle with wavelength toward KL than along the ridge between KL and KHW is also clearly seen when the data are compared with observations at 850 μm (not shown, but see, e.g., Matthews et al. 2003).

The color scale of Figure 1*c* shows the ratio of the polarization amplitude at the two wavelengths, *P*(450)/*P*(350). Most points in the map exhibit a two-point polarization spectrum which increases with wavelength, *P*(450)/*P*(350) > 1 (Fig. 2). The most obvious exceptions are toward KL and the region to its northwest. KHW does not exhibit a similar drop in the polarization ratio.

4. DISCUSSION

4.1. *Minimum in the Polarization Spectrum*

In order to avoid effects related to opacity, previous studies of far-infrared and submillimeter polarization spectra have been restricted to regions outside of flux peaks (e.g., Hildebrand et

[9] See http://www.submm.caltech.edu/~sharc/analysis/overview.htm.
[10] See http://www.submm.caltech.edu/~sharc/analysis/calibration.htm.

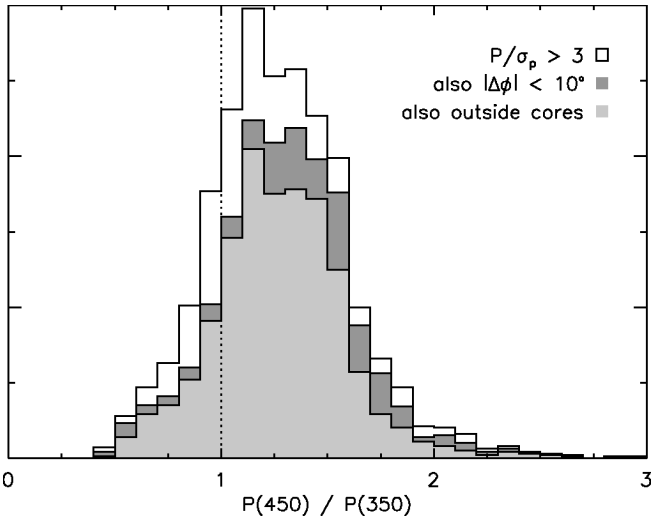

FIG. 2.—Histogram of the 450 μm/350 μm polarization ratio. All data shown here have been limited to only those points where $P \geq 3\sigma_p$ at both wavelengths. Also shown are histograms where data points satisfy the additional criteria that the position angle rotate by less than 10° between the two wavelengths ($|\Delta\phi| < 10°$) and that the points be at least 20″ away from the two submillimeter flux density peaks KL and KHW.

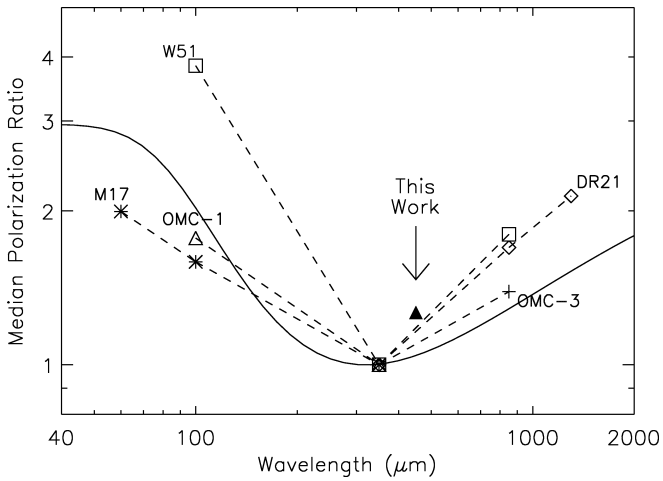

FIG. 3.—Far-infrared and submillimeter polarization spectrum, normalized at 350 μm. The 450 μm/350 μm OMC-1 comparison from this work is shown as a filled triangle. The 850 μm/350 μm comparison in W51 (*open squares*) uses data at 850 μm from Chrysostomou et al. (2002) and 350 μm data from Dotson et al. (2008). This ratio is calculated in the same manner as for all other data points, which are from Vaillancourt (2002). The solid curve is a two-component dust model (see text).

al. 1999; Vaillancourt 2002). Such studies are further restricted to regions where the polarization position angle varies by less than 10° between wavelengths. This last restriction limits the effects a line-of-sight-varying magnetic field might have on the measured plane-of-sky polarization. The histograms in Figure 2 show the distribution of the polarization ratio $P(450)/P(350)$ for all the data shown in Figure 1 as well as the resulting distributions after the above-discussed cuts are applied.

For data which lie outside the two flux peaks (beyond a 20″ radius), and also satisfy the 10° cut, we find a median in the distribution of $P(450)/P(350) = 1.3 \pm 0.3$ (where the uncertainty represents the standard deviation of those points). This ratio is plotted in Figure 3 along with measurements from other Galactic clouds. The $P(450)/P(350)$ ratio measured here is consistent with a simple interpolation of the previous measurements. From the results of Figure 3, and assuming that the polarization spectrum in OMC-1 is similar to that of other clouds (i.e., it continues to rise at wavelengths greater than 450 μm), we conclude that the minimum in the spectrum must fall in the range 100–350 μm.

4.2. *Polarization Ratio in Different Environments*

Given the low polarization ratio toward KL compared with the rest of the cloud, it is natural to ask whether this may be due to some unique physical condition as compared with the remainder of the cloud. At the very least, it is obvious that KL is the region with the highest flux density in the cloud. To examine this trend, we plot the 450/350 polarization ratio as a function of 350 μm flux density F_{350}. Figure 4 plots the polarization data as individual points (*dots*) and combined into equal-sized logarithmic flux density bins (*diamonds*). At low flux densities ($F_{350} \lesssim 50\%$ of the peak) the polarization ratio clusters about $P(450)/P(350) \approx 1.2$–1.5 with a large scatter (this distribution is best shown in the histogram of Fig. 2). At $F_{350} \gtrsim 50\%$ the binned data show a sharp drop in the polarization ratio. The flux density at which this drop occurs is indicated by the thick contours in Figure 1*c*. With few exceptions all data above this flux density level lie in KL. The binned data in Figure 4 drop below $P(450)/P(350) = 1$ for $F(350) \gtrsim 60\%$. At this flux density level all points are within ~20″ of KL.

Polarized emission from dust grains all with the same temperature results in a nearly constant polarization spectrum in the wavelength range 50–2000 μm (Hildebrand et al. 1999). The polarization spectrum in Figure 3 requires the existence of at least two dust-emission components (Hildebrand et al. 1999; Vaillancourt 2002); such a spectrum is modeled in the figure. This model has a minimum at 330 μm and uses optically thin dust with temperatures $T = 20$ and 50 K, spectral indices $\beta = 2$ and 1, respectively,[11] and peak flux densities in the ratio $F_{\rm cold}/F_{\rm hot} = 0.5$. The cold component is unpolarized while the

[11] An inverse T-β relation is observed to be typical for dust in molecular clouds (e.g., Dupac et al. 2001, 2003).

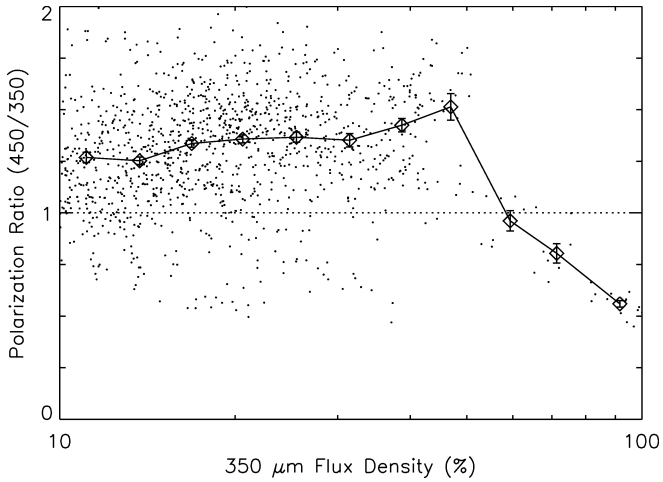

FIG. 4.—Polarization ratio (450 μm/ 350 μm) vs. the total 350 μm flux density (percentage of peak ≈780 Jy per 9″ beam). Dots indicate individual measurements within the maps of Fig. 1*c* while diamonds represent an average of the plotted quantity over logarithmic bins of 350 μm flux density. Error bars on the polarization ratio represent the standard deviation of the mean within each bin.

warm component is polarized. While a two-component dust model for molecular clouds is physically unrealistic, it is sufficient to illustrate how a multicomponent model can explain the empirical results.

Even with only two components, small adjustments to the parameters allow for better agreement between the model and the specific data points of Figure 3. A spectral energy distribution (SED) dominated by cold unpolarized dust ($F_{\rm cold}/F_{\rm hot} \gg 1$) can reproduce the ratio observed in the OMC-1 cloud envelope, $P(450)/P(350) \approx 1.3$. Such an SED will appear nearly isothermal if the measurement uncertainties are large and/or it is not sufficiently sampled in wavelength space. This is consistent with the SED analysis of Vaillancourt (2002) in which no significant evidence is seen for multiple dust temperatures outside of KL or the M42 H II region, but where the polarization spectrum is still observed to change with wavelength.

This same SED study found that the KL region contains high column densities of both warm ($T \approx 45$ K) and cold ($T \approx 20$ K) dust which contribute nearly equally to the total flux density observed at 350 and 450 μm. As one moves toward KL from within 30″ of the peak the temperature of the cold component decreases by ~2 K, and the warm component increases by ~3 K. These modest temperature changes are enough to shift the polarization minimum by as much as 70–130 μm (depending on the relative spectral indices of the components), moving to longer wavelengths toward the intensity peak.

Therefore, we expect the polarization minimum to shift to longer wavelengths at the KL peak. If the observed wavelengths are near the minimum then we expect the 450/350 polarization ratio to decrease from a value greater than unity when the minimum is below 400 μm, to a value approximately equal to one when the minimum is bracketed by the two observed wavelengths, and to continue to decrease below one as the minimum moves to wavelengths greater than 400 μm. This is the trend observed in Figure 4 for points with $F_{350} \gtrsim 50\%$.

5. SUMMARY AND FUTURE WORK

By comparing the 450 μm/350 μm polarization ratio in OMC-1 with that in other bright Galactic clouds (Fig. 3) we estimate that the minimum of the polarization spectrum in the OMC-1 envelope (outside of the KL and KHW flux density peaks) occurs at wavelengths between 100 and 350 μm. However, given the variation in the 60–1300 μm polarization spectrum from cloud to cloud, we do not draw strong conclusions about the polarization minimum in any cloud other than OMC-1. We are continuing our campaign to observe and analyze other bright clouds in a manner similar to that described here.

The existence of a minimum in the far-infrared/submillimeter polarization spectrum, as opposed to a simple rise or fall from one end of the spectrum to the other, implies either (1) the existence of at least two dust temperature components, and/or (2) a change in the dust emissivity index as well as its temperature. Multiwavelength observations in the far-infrared (50–200 μm; Dotson et al. 2000; Dowell et al. 2003; Vaillancourt et al. 2007) or submillimeter (>450 μm; Curran & Chrysostomou 2007; Bastien et al. 2005; B. C. Matthews et al., in preparation) at wavelengths on only one side of this minimum are insufficient for studying this behavior. SHARP (at 350 and 450 μm) therefore occupies a unique niche for studies of the polarization spectrum by providing a link between these two wavelength extremes.

We are grateful for the help of the Caltech Submillimeter Observatory (CSO) staff in installing and observing with SHARP and SHARC-II. Also thanks to Jackie Davidson, and Emeric Le Floc'h for observing assistance. SHARP has been supported by NSF grants AST 02-41356, AST 05-05230, and AST 05-05124. The CSO is supported by the NSF through grant AST 05-40882.

Facilities: CSO(SHARC2)

REFERENCES

Andersson, B-G, & Potter, S. B. 2007, ApJ, 665, 369
Bastien, P., Jenness, T., & Molnar, J. 2005, in ASP Conf. Ser. 343, Astronomical Polarimetry, ed. A. Adamson et al. (San Francisco: ASP), 69
Chrysostomou, A., Aitken, D. K., Jenness, T., Davis, C. J., Hough, J. H., Curran, R., & Tamura, M. 2002, A&A, 385, 1014
Coppin, K. E. K., Greaves, J. S., Jenness, T., & Holland, W. S. 2000, A&A, 356, 1031
Curran, R. L., & Chrysostomou, A. 2007, MNRAS, 382, 699
Dotson, J. L., Davidson, J. A., Dowell, C. D., Hildebrand, R. H., Kirby, L., & Vaillancourt, J. E. 2008, ApJS, submitted
Dotson, J. L., Davidson, J., Dowell, C. D., Schleuning, D. A., & Hildebrand, R. H. 2000, ApJS, 128, 335
Dowell, C. D., Davidson, J. A., Dotson, J. L., Hildebrand, R. H., Novak, G., Rennick, T. S., & Vaillancourt, J. E. 2003, Proc. SPIE 4843, 250
Dupac, X., et al. 2001, ApJ, 553, 604
———. 2003, A&A, 404, L11
Hildebrand, R., & Kirby, L. 2004, in ASP Conf. Ser. 309, Astrophysics of Dust, ed. A. N. Witt, G. C. Clayton, & B. T. Draine (San Francisco: ASP), 515
Hildebrand, R. H., Davidson, J. A., Dotson, J. L., Dowell, C. D., Novak, G., & Vaillancourt, J. E. 2000, PASP, 112, 1215
Hildebrand, R. H., Dotson, J. L., Dowell, C. D., Schleuning, D. A., & Vaillancourt, J. E. 1999, ApJ, 516, 834
Hildebrand, R. H., & Dragovan, M. 1995, ApJ, 450, 663
Houde, M., Dowell, C. D., Hildebrand, R. H., Dotson, J. L., Vaillancourt, J. E., Phillips, T. G., Peng, R., & Bastien, P. 2004, ApJ, 604, 717
Houde, M., & Vaillancourt, J. E. 2007, PASP, 119, 871
Johnstone, D., & Bally, J. 1999, ApJ, 510, L49
Keene, J., Hildebrand, R. H., & Whitcomb, S. E. 1982, ApJ, 252, L11
Lazarian, A. 2003, J. Quant. Spectrosc. Radiat. Transfer, 79, 881
———. 2007, J. Quant. Spectrosc. Radiat. Transfer, 106, 225
Li, H., Attard, M., Dowell, C. D., Hildebrand, R. H., Houde, M., Kirby, L., Novak, G., & Vaillancourt, J. E. 2006, Proc. SPIE, 6275, 48
Li, H., Dowell, C. D., Kirby, L., Novak, G., & Vaillancourt, J. E. 2008, Appl. Optics, 47, 422
Lis, D. C., Serabyn, E., Keene, J., Dowell, C. D., Benford, D. J., Phillips, T. G., Hunter, T. R., & Wang, N. 1998, ApJ, 509, 299
Martin, P. G., Clayton, G. C., & Wolff, M. J. 1999, ApJ, 510, 905
Martin, P. G., & Whittet, D. C. B. 1990, ApJ, 357, 113
Matthews, B. C., Chuss, D., Dotson, J., Dowell, D., Hildebrand, R., Johnstone, D., & Vaillancourt, J. 2003, in Chemistry as a Diagnostic of Star Formation, ed. C. L. Curry & M. Fich (Ottawa: NRC Press), 145
Matthews, B. C., Wilson, C. D., & Fiege, J. D. 2001, ApJ, 562, 400
Novak, G., et al. 2004, Proc. SPIE, 5498, 278
Platt, S. R., Hildebrand, R. H., Pernic, R. J., Davidson, J. A., & Novak, G. 1991, PASP, 103, 1193
Roberge, W. G. 2004, in ASP Conf. Ser. 309, Astrophysics of Dust, ed. A. N. Witt, G. C. Clayton, & B. T. Draine (San Francisco: ASP), 467
Schleuning, D. A. 1998, ApJ, 493, 811
Serkowski, K. 1958, Acta Astron., 8, 135
Simmons, J. F. L., & Stewart, B. G. 1985, A&A, 142, 100
Vaillancourt, J. E. 2002, ApJS, 142, 53
———. 2006, PASP, 118, 1340
———. 2007, in Sky Polarisation at Far-infrared to Radio Wavelengths, ed. F. Boulanger & M.-A. Miville-Deschênes (EAS Publ. Ser. 23; Les Ulis: EDP Sciences), 147
Vaillancourt, J. E., et al. 2007, Proc. SPIE, 6678, 66780D
Whittet, D. C. B. 2004, in ASP Conf. Ser. 309, Astrophysics of Dust, ed. A. N. Witt, G. C. Clayton, & B. T. Draine (San Francisco: ASP), 65
Whittet, D. C. B., Hough, J. H., Lazarian, A., & Hoang, T. 2008, ApJ, 674, 304